AIMS Materials Science, 5(4): 624–649.
DOI: 10.3934/matersci.2018.4.624
Received: 15 May 2018
Accepted: 22 July 2018
Published: 01 August 2018

http://www.aimspress.com/journal/Materials

Research article

Prediction of first-year corrosion losses of copper and aluminum in continental regions

Yulia M. Panchenko*, Andrey I. Marshakov, Ludmila A. Nikolaeva and Victoria V. Kovtanyuk

A.N.Frumkin Institute of Physical Chemistry and Electrochemistry, Russian Academy of Sciences, Moscow, 119071, Russia

*** Correspondence:** Email: panchenkoyum@mail.ru.

Abstract: The dose-response functions (DRFs) developed for the prediction of first-year corrosion losses of copper and aluminum (K_1) in continental regions are presented. The development of DRFs is based on the stablished dependences of the corrosion losses of these metals on SO_2 concentration: $K = f([SO_2])$. Experimental data on the atmosphere corrosivity and corrosion losses of the metals in a one-year exposure period according to ISOCORRAG and UN/ECE international programs, the Russian program, and MICAT project were used. Comparisons of the predicted K_1 values obtained by three different DRFs with experimental K_1 values are presented. These DRFs are analyzed in terms of the coefficients they contain.

Keywords: copper; aluminum; modelling; atmospheric corrosion

1. Introduction

The atmospheric corrosion of metal systems is among the common types of degradation of structural materials. The corrosion mass loss or depth of corrosion damage depends on the atmosphere corrosivity and varies in a broad range under real conditions of each atmosphere type. According to the experimental data of one-year corrosion tests under the ISO CORRAG [1] and UNECE international programs [2,3], MICAT project [4,5] and the Russian program [6], in

continental regions of the world the ranges of first-year corrosion losses are 5.4–685 g/m^2 for carbon steel, 0.65–38.4 g/m^2 for zinc, 0.76–18.31 g/m^2 for copper, and 0.027–2.57 g/m^2 for aluminum. Taking into account the considerable difference in the corrosion resistance of metals in the atmosphere, the design of metal structures and their protection from atmospheric corrosion require data on the atmosphere corrosivity category and corrosion mass losses in various climate zones and atmosphere types over various periods of time. The K_1 value is an important parameter: a) based on K_1, the atmosphere corrosivity categories are estimated [7]; b) K_1 values are used for long-term predictions of corrosion mass losses of metals, e.g., see [8–16]. The power-linear [17] and power [18,19] functions for the prediction of corrosion mass losses in any world regions are based on K_1 values predicted using DRFs (K_1^{pr}) [18–20]. The K_1^{pr} values at any location should match the long-time annual average meteorological and aerological atmosphere parameters. An advantage of DRFs is that they make it unnecessary to perform numerous one-year exposures at every location in order to obtain valid mean K_1 values corresponding to the current natural conditions.

All the DRFs were developed using regression analysis, with consideration for the identified or assumed regularities of the effect of separate atmosphere corrosivity parameters on the corrosion. Therefore, they can have various mathematical forms. Currently, no model is perfect due to, at least, the following factors: a) imprecise mathematical form of the DRFs; b) imprecise values of the coefficients that are used in the DRFs and are calculated from regression analysis; c) incomplete set of atmosphere corrosivity parameters that affect corrosion [20]. Therefore, DRFs can be improved based on the gained knowledge about the effect of each atmosphere corrosivity parameter on the corrosion.

The DRFs for carbon steel and zinc [7] developed for various world regions have nearly the same mathematical form for K_1 prediction. The results of K_1 predictions for continental regions using these models differ considerably, as shown in [18,21]. This is due to the difference in the coefficients used in these DRFs. Ref [21] presents new DRFs for these metals based on the $K = f([SO_2])$ relationship obtained, and gives a comparative estimate of the values of the coefficients in the DRFs.

The purpose of this paper is to obtain the $K = f([SO_2])$ relationships for copper and aluminum and to develop new DRFs for K_1 predictions on these metals based on the $K = f([SO_2])$ relationship coefficients and meteorological parameters of atmosphere corrosivity obtained. Yet another purpose is to give a comparison of K_1 predictions for these metals based on the new and earlier DRFs [7,18] for continental territories of the world, and to analyze the coefficients in these DRFs.

2. Procedure

2.1. Development of DRFs for continental territories

The corrosion of metals is affected by numerous factors that currently cannot all be taken into account. Therefore, in order to develop a DRF, one primarily needs to choose its mathematical form and the atmosphere parameters that affect corrosion most strongly. As a rule, two main parameters were taken into account for the prediction of metal corrosion in continental regions: SO_2 concentration in air and time of wetting (*TOW*) of the metal surface. The relationship was studied between the *TOW*, on the one hand, and the mean annual temperature (*T*) and air relative humidity

(*RH*), on the other hand. It was shown that the temperature dependence of the time of surface wetting (at *RH* > 80% and *T* > 0 ℃) has a maximum around *T* = +10…+13 ℃ [22,23]. In view of this, it was suggested to describe the temperature dependence of metal corrosion rate in two ranges, $T \le T_{lim}$ and $T > T_{lim}$, by simple relationships of ln(*K* − *T*) type. T_{lim} is the temperature corresponding to the maximum *K* values. The boundary between the ranges, T_{lim}, is not necessarily the same as the maximum in the *TOW*—temperature plot due to complex changes in the state of the adsorbed water layers that also depend on *T* [22,24]. The temperature dependence of corrosion for the majority of metals has a maximum in the range of *T* = +9…+11 ℃ [22]. The plot of *K* versus *RH* is close to an exponent if the *RH* range is sufficiently wide. In development of the new DRFs, the main attention was given to the determination of the relationship between the corrosion losses of copper and aluminum, on the one hand, and the concentration of sulfur dioxide in air, on the other hand.

To develop the DRFs, we used experimental data from all exposures over the first test year in continental regions with in the MICAT [4,5] (8 countries, 26 locations, copper and aluminum tests) and UN/ECE [2,3] international programs (11 countries, 27 locations, copper tests) and the Russian program [6] (12 locations, copper and aluminum tests). The background chloride precipitation at the locations did not exceed 1.5 g/(m^2 day). The test locations (country, location name, code), atmosphere corrosivity parameters, and experimental K_1 values obtained from 1–3 one-year exposures are resented in Tables 1–3. The test results obtained under the ISO CORRAG program [1] are not provided in this paper because they lack the atmosphere corrosivity parameters required for K_1 prediction. We used them only to find the $K = f([SO_2])$ dependences for copper and aluminum.

Table 1. UN/ECE program. Test locations, atmosphere corrosivity parameters, K_1 (g/m^2) of copper from one-year exposures, and location numbers in the order of increasing K_1.

Country	Test location	Designation	*T*, °C	*RH*, %	O_3, μg/m^3	*Prec*, mm/y	SO_2, μg/m^3	H^+, mg/L	Cu	
									K_1, g/m^2	No.
Czech Republic	Prague	CS1	9.5	79	-	639.3	77.5	0.1	10.87	13
	Kasperske Hory	CS2	7.0	77	-	850.2	19.7	0.1	15.04	22
	Kopisty	CS3	9.6	73	-	426.4	83.3	0	27.59	27
Finland	Espoo	FIN4	5.9	76	-	625.9	18.6	0.1	7.44	10
	Ähtäri	FIN5	3.1	78	52	801.3	6.3	0	11.87	18
	Helsinki Vallila	FIN6	6.3	78	-	673.1	20.7	0	5.89	6
Germany	Waldhof Langenbrügge	GER7*	9.3	80	59	630.6	13.7	0.1	15.78	24
	Aschaffenburg	GER8	12.3	77	27	626.9	23.7	0	6.05	7
	Langenfeld Reusrath	GER9	10.8	77	30	782.9	24.5	0	6.95	9
	Bottrop	GER10	11.2	75	-	873.8	50.6	0	11.71	17
	Essen Leithe	GER11	10.5	79	-	713.1	30.3	0	9.06	11
	Garmisch Partenkirchen	GER12	8.0	82	50	1491.5	9.4	0	11.42	15
Netherlands	Eibergen	NL18	9.9	83	40	904.2	10.1	0.0036	13.37	19
	Vredepeel	NL19	10.3	81	36	845	13	0.0048	16.79	25
	Wijnandsrade	NL20	10.3	81	39	801.3	13.7	0.0188	13.92	20
Norway	Oslo	NOR21	7.6	70	-	1023.8	14.4	0.0334	6.95	8
	Birkenes	NOR23	6.5	80	60	2144.3	1.3	0.0567	10.97	14
Sweden	Stockholm South	SWE24	7.6	78	44	531	16.8	0.045	5.33	5
	Stockholm Centre	SWE25	7.6	78	-	531	19.6	0.045	4.40	4
	Aspvreten	SWE26	6.0	83	55	542.7	3.3	0.0541	10.71	12
Spain	Madrid	SPA31	14.1	66	26	398	18.4	0.0055	3.12	1
	Toledo	SPA33	14.0	64	77	785	3.3	0.0054	3.54	2
Russian Federation	Moscow	RUS34	5.5	73	-	575.4	19.2	0.0007	4.14	3
Estonia	Lahemaa	EST35	5.5	83	-	447.8	0.9	0.0221	11.47	16

Continued on next page

Country	Test location	Designation	*T*, ℃	*RH*, %	O_3, μg/m^3	*Prec*, mm/y	SO_2, μg/m^3	H^+, mg/L	Cu	
									K_1, g/m^2	No.
Canada	Dorset	CAN37	5.5	75	59	961.1	3.3	0.0541	14.68	21
USA	Research Triangle Park	US38	14.6	69	54	846.7	9.6	0.0517	15.48	23
	Steubenville	US39	12.3	67	42	733.1	58.1	0.1008	18.96	26

* The concentration of chloride the in precipitations was [Cl^-] = 3.92 mg/L.

Table 2. MICAT program. Test locations, atmosphere corrosivity parameters, K_1 (g/m^2) of copper and aluminum from one-year exposures, and location numbers in the order of increasing K_1.

Country	Test location	Designation	*T*, ℃	*RH*, %	*Rain*, mm/y	SO_2, μg/m^3	Cl^-, mg/(m^2 d)	Cu		Al	
								K_1, g/m^2	No.	K_1, g/m^2	No.
Argentina	Villa Martelli	A2	16.7	75	1729	10	Ins	7.23	29	0.378	30
		A2	17.1	72	983	10	Ins	5.63	20	0.216	18
		A2	17.0	74	1420	9	Ins	8.30	37	0.405	32
	Iguazu	A3	20.6	76	2158	Ins	Ins	0.82	*	0.27	*
		A3	20.9	74	2624	Ins	Ins	0.81	*	0.567	*
		A3	22.1	75	1720	Ins	Ins	0.7	*	0.756	*
	San Juan	A4	18.0	51	35	Ins	Ins	1.70	5	0.162	15
		A4	20.0	49	111	Ins	Ins	1.43	2	0.405	31
		A4	18.3	51	93	Ins	Ins	1.52	3	0.108	12
	La Plata	A6	17.0	78	1178	6.22	Ins	11.79	41	0.351	25
		A6	16.7	77	1263	8.21	Ins	15.63	46	0.54	35
		A6	16.6	78	1361	6.2	Ins	14.56	45	0.324	23
Brasil	Caratinga	B1	21.2	75	996	1.67	1.57	1.09	*	0.297	*
	Sao Paulo	B6	19.7	75	1409	67.2	Ins	18.31	47	1.836	40
		B6	19.5	76	1810	66.8	Ins	14.29	44	1.458	39
		B6	19.6	75	1034	48.8	Ins	12.59	43	1.242	38

Continued on next page

Country	Test location	Designation	*T*, ℃	*RH*, %	*Rain*, mm/y	SO_2, μg/m^3	Cl^-, mg/(m^2 d)	Cu		Al	
								K_1, g/m^2	No.	K_1, g/m^2	No.
Brasil	Belem	B8	26.1	88	2395	Ins	Ins	5.72	21	0.594	
	Brasilia	B10	20.4	69	1440	Ins	Ins	1.12	*	0.729	*
	Paulo Afonso	B11	25.9	77	1392	Ins	Ins	1.86	*	1.485	*
	Porto	B12	26.6	90	2096	Ins	Ins	1.94	*	-	-
Colombia	Cotove	CO2	9.6	98	1800	0.56	Ins	9.56	38	0.432	33
		CO2	11.4	90	1800	0.56	Ins	8.13	36	0.648	36
		CO2	13.5	81	1800	0.56	Ins	10.36	40	-	-
	Guayaquil	CO3	27.0	76	900	0.33	Ins	0.73	*	-	-
		CO3	27.0	76	900	0.33	Ins	0.63	*	0.378	*
		CO3	27.0	76	900	0.33	Ins	0.94	*	-	-
Ecuador	Riobamba	EC1	26.1	71	635	4.2	1.5	5.89	22	0.081	9
		EC1	26.9	82	635	2.72	1.31	6.43	25	0.081	10
		EC1	24.8	75	564	2.1	1.66	6.79	26	-	-
	Leon	EC2	12.9	66	554	1.0	0.4	3.21	9	-	-
		EC2	13.2	71	598	1.35	1.14	4.38	15	-	-
Spain	Tortosa	E1	12.0	69	652	1.18	1.5	9.73	39	0.378	26
		E1	10.6	65	495	1.18	1.5	7.95	35	0.297	20
		E1	11.1	63	334	1.18	1.5	4.11	12	0.378	27
	Granada	E4	18.1	65	554	8.3	1.5	6.79	27	0.297	21
		E4	17.0	63	521	5.7	1.5	7.41	30	0.135	14
		E4	17.2	62	374	1.9	1.5	7.59	32	0.216	16
	Arties	E5	16.3	59	416	10.3	1.5	2.51	*	0.135	*
		E5	15.0	59	258	5.4	1.5	1.97	*	0.081	*
		E5	15.6	58	266	2.8	1.5	1.34	*	0.081	*
		E8	8.8	52	738	9.1	1.8	5.54	19	0.378	29
		E8	6.9	52	624	8.9	1.6	4.73	16	0.216	17

Continued on next page

Country	Test location	Designation	*T*, ℃	*RH*, %	*Rain*, mm/y	SO_2, μg/m^3	Cl^-, mg/(m^2 d)	Cu		Al	
								K_1, g/m^2	No.	K_1, g/m^2	No.
Spain	Arties	E8	7.8	52	681	9.0	1.7	6.25	24	0.324	24
Mexico	Mexico (a)	M1	15.1	63	743	14.9	1.5	5.36	18	0.432	34
		M1	14.6	63	743	17.6	1.5	7.50	31	0.216	19
		M1	15.6	63	743	3.5	1.5	4.29	14	-	-
	Mexico (b)	M2	21.0	56	1352	6.7	1.5	2.05	7	0.378	28
		M2	21.0	56	1724	9.9	Ins	2.50	8	0.297	22
		M2	21.0	56	1372	7.1	Ins	3.57	10	1.242	37
	Cuernavaca	M3	18.0	51	374	31.1	Ins	5.98	23	-	-
		M3	18.0	62	374	10.9	Ins	4.29	13	1.674	*
		M3	18.0	60	374	14.6	Ins	3.84	11	1.242	*
Peru	San Luis Potosi	PE4	16.4	37	17	Ins	Ins	1.70	4	0.027	1
		PE4	17.2	33	34	Ins	Ins	1.79	6	0.027	2
	Arequipa	PE5	12.2	67	632	Ins	Ins	0.81	1	0.027	3
		PE5	12.2	67	672	Ins	Ins	-	-	0.081	8
	Arequipa	PE6	25.4	84	1523	Ins	Ins	5.00	17	0.108	11
		PE6	25.8	83	1158	Ins	Ins	-	-	0.027	4
Uruguay	Pucallpa	U1	16.8	74	1182	0.6	1.8	7.05	28	0.027	5
		U1	16.6	73	1324	0.8	1.2	7.59	34	0.027	6
		U1	16.7	76	1306	Ins	Ins	7.59	33	0.054	7
	Trinidad	U3	17.7	79	1490	Ins	Ins	11.97	42	0.108	13

* discarded data.

Table 3. Test locations, atmosphere corrosivity parameters, K_1 (g/m^2) of copper and aluminum from one-year exposures, and location numbers in the order of increasing K_1.

Location	*T*, ℃	*RH*, %	*Prec*, mm/y	SO_2, μg/m^3	Cu		Al	
					K_1, g/m^2	No.	K_1, g/m^2	No.
Bilibino	−12.2	80	218	3	0.84	2	0.177	2
Oimyakon	−16.6	71	175	3	0.76	1	0.189	3
Ust-Omchug	−11	70	317	5	0.92	3	0.242	5
Atka	−12	72	376	3	0.98	4	0.164	1
Susuman	−13.2	71	283	10	1.37	5	0.474	12
Tynda	−6.5	72	525	5	1.62	6	0.280	8
Klyuchi	1.4	69	253	3	2.82	10	0.310	11
Aldan	−6.2	72	546	5	1.78	7	0.205	4
Pobedino	−0.9	77	604	3	6.69	12	0.285	10
Yakovlevka	2.5	70	626	3	4.06	11	0.259	7
Pogranichnyi	3.6	67	595	3	2.79	9	0.258	6
Komsomolsk-on-Amur	−0.7	76	499	10	2.45	8	0.285	9

2.2. Predictions of first-year corrosion losses

The corrosion losses for the first year of exposure (K_1) were predicted for continental test locations at background Cl^- precipitation ≤1.5 mg/(m^2 day). The DRFs presented in this article (hereinafter referred to as New DRF), in the Standard [7] (hereinafter—Standard DRF), and in Ref [18] (hereinafter—Unified DRF) were used.

The standard DRFs are intended for the prediction of K_1 (r_{corr} in the original, μm) for two temperature ranges.

For copper, Eq 1:

$$K_1 = 0.0053 \cdot P_d^{0.26} \exp(0.059 \cdot RH + f_{Cu}) + 0.01025 \cdot S_d^{0.27} \exp(0.036 \cdot RH + 0.049 \cdot T),$$
$$f_{Cu} = 0.126 \cdot (T - 10) \text{ at } T \le 10\ ℃; f_{Cu} = -0.080(T - 10) \text{ at } T > 10\ ℃ \quad (1)$$

For aluminum, Eq 2:

$$K_1 = 0.0042 \cdot P_d^{0.73} \exp(0.025 \cdot RH + f_{Al}) + 0.0018 \cdot S_d^{0.60} \exp(0.020 \cdot RH + 0.094 \cdot T),$$
$$f_{Al} = 0.009 \cdot (T - 10) \text{ at } T \le 10\ ℃; f_{Al} = -0.043 \cdot (T - 10) \text{ at } T > 10\ ℃ \quad (2)$$

where T is the temperature (℃) and RH (%) is the relative humidity of air; P_d and S_d are the SO_2 and Cl^- deposition rates expressed in mg/(m^2 day), respectively.

In Eqs 1 and 2, the contributions to corrosion due to SO_2 and Cl^- are presented as separate components, therefore only their first components were used for continental territories.

The Unified DRFs are intended for long-term predictions of mass losses K (designated as *ML* in the original). It is stated that the calculated values are given in g/m^2.

For copper, Eq 3:

$$K = 0.0027\ [SO_2]^{0.32}\ [O_3]^{0.79}\ RH\ \exp\{+0.083\ (T-10)\}\cdot\tau^{0.78} + 0.050\ Rain\ [H^+]\cdot\tau^{0.89},\ T \le 10\ ^\circ C;$$
$$K = 0.0027\ [SO_2]^{0.32}\ [O_3]^{0.79}\ RH\cdot\exp\{-0.032\ (T-10)\}\cdot\tau^{0.78} + 0.050\ Rain\ [H^+]\cdot\tau^{0.89},\ T > 10\ ^\circ C \quad (3)$$

For aluminum, Eq 4:

$$K = 0.0021\ [SO_2]^{0.23}\ RH\ \exp\{+0.031\ (T-10)\}\cdot\tau^{1.2} + 0.000023\ Rain\ [Cl^-]\cdot\tau,\ T \le 10\ ^\circ C;$$
$$K = 0.0021\ [SO_2]^{0.23}\ RH\cdot\exp\{-0.061\cdot(T-10)\}\cdot\tau^{1.2} + 0.000023\ Rain\ [Cl^-]\cdot\tau,\ T > 10\ ^\circ C \quad (4)$$

where $[SO_2]$ is the concentration of SO_2, μg/m^3; *Rain* is the rainfall amount, mm/y; $[H^+]$ is the acidity of the precipitations; $[O_3]$ is the ozone concentration in the air, μg/m^3; $[Cl^-]$ is the concentration of chlorides in rain water, mg/L; and τ is the exposure time, years.

To predict the first-year corrosion losses, τ = 1 was taken.

The K_1 values in μm were converted to g/m^2 using the specific densities of copper and aluminum equal to 8.96 and 2.7 g/cm^3, respectively. Furthermore, the relationship $P_{d,p} = 0.67\ P_{d,c}$ was used, where $P_{d,p}$ (mg/(m^2 day)) is the SO_2 deposition rate and $P_{d,c}$ (μg/m^3) is the SO_2 concentration [7].

The $K = f([SO_2])$ relationship is nonlinear, therefore the background SO_2 concentrations at the test locations cannot be smaller than 1 μg/m^3, since at $[SO_2] < 1$ μg/m^3 the calculated K_1 values would be smaller than the experimental K_1. In our calculations, we used the value of 1 μg/m^3 for SO_2 concentrations indicated in Tables 1 and 2 as "Ins." or ≤1 μg/m^3, whereas the remaining SO_2 concentrations were taken from the Tables.

The K_1 predictions obtained by different DRFs are compared to the experimental K_1 values for each test location, which provides a clear idea about the specific features of predictions by each DRF.

3. Results and discussion

3.1. Development of New DRFs

To develop a DRF, it is first of all necessary to estimate the effect of sulfur dioxide on corrosion, i.e., find the mathematical relationship $K = f([SO_2])$. The estimate was based on actual data on K_1 and SO_2 concentrations from all one-year exposures under each of the programs.

Despite the considerable scatter of experimental K_1 values (Figures 1 and 2) obtained in broad ranges of meteorological atmosphere parameters, it is evident that, in a first approximation, this relationship can be described by a function that has the form:

$$K_1 = \check{K}_1^0\ [SO_2]^{\alpha} \quad (5)$$

where $\check{K}_1^0$ is the mean value of the first-year corrosion losses (g/m^2) in a pure atmosphere and α is the exponent that depends on the metal nature.

Selection of $\check{K}_1^0$ values proved to be complicated due to a scatter in the experimental K_1^0 values in a pure atmosphere. An inaccurate $\check{K}_1^0$ value would result in an inaccurate estimate of the α value that is used in the DRF. We chose the $\check{K}_1^0$ values of 3 and 0.1 g/m^2 and the α values of 0.38 and 0.67 for copper and aluminum, respectively, as the most suitable values for the averaged description of the

experimental data. The $K = f([SO_2])$ relationships obtained for each program based on the selected $\check{K}_1^0$ и α values are shown in Figure 1 for copper and in Figure 2 for aluminum. In a first approximation, the lines of the relationships obtained pass through the mean experimental points.

In the development of the New DRF, the K_1 values for copper and aluminum were determined using the mathematical form of the New DRFs developed for carbon steel and zinc. The *Prec* parameter, including *Rain* and solid precipitation, was introduced in the DRFs [21]. DRFs were also developed for two temperature ranges.

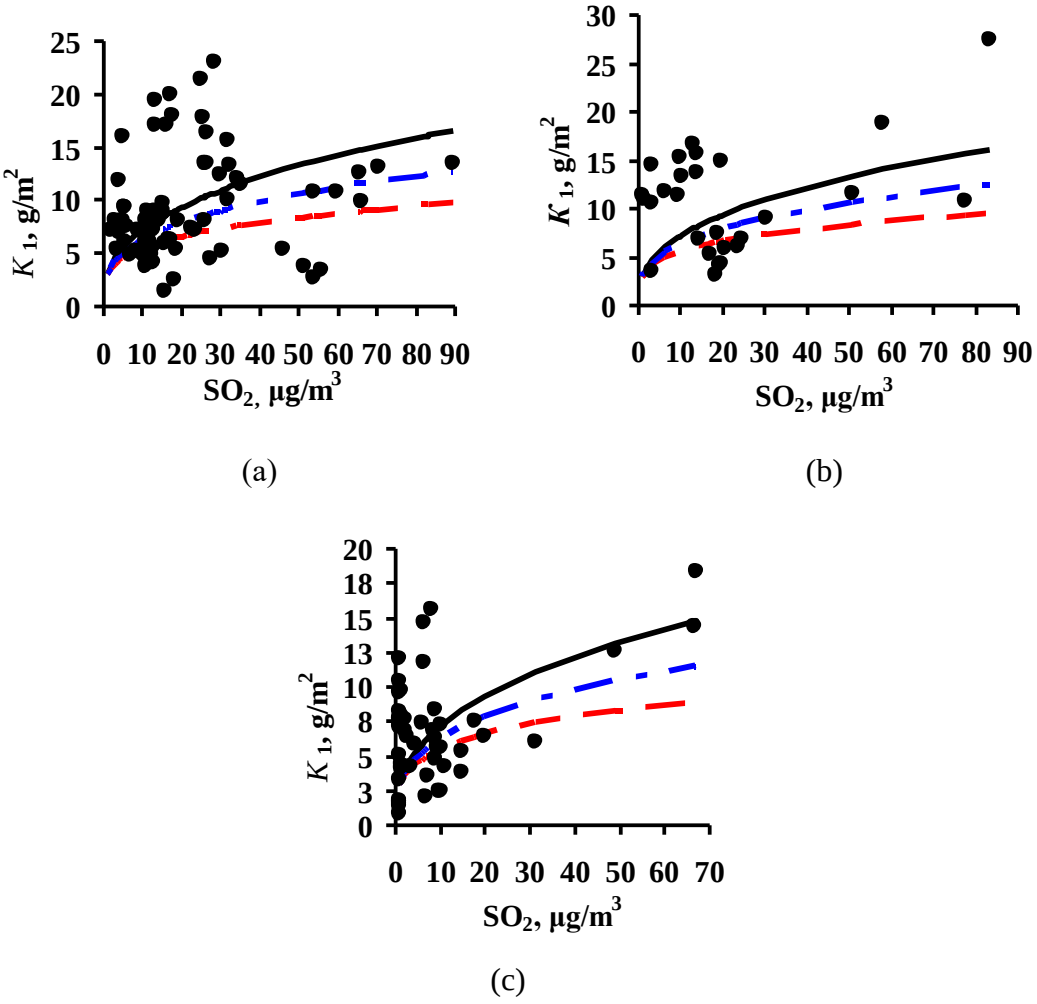

Figure 1. Plot of the first-year corrosion losses of copper (K_1) on SO_2 concentration based on the data from ISO CORRAG program (a), UN/ECE program (b), and MICAT project (c). ——: α = 0.38 (New DRF), — —: α = 0.26 (Standard DRF), — ● —: α = 0.32 (Unified DRF).

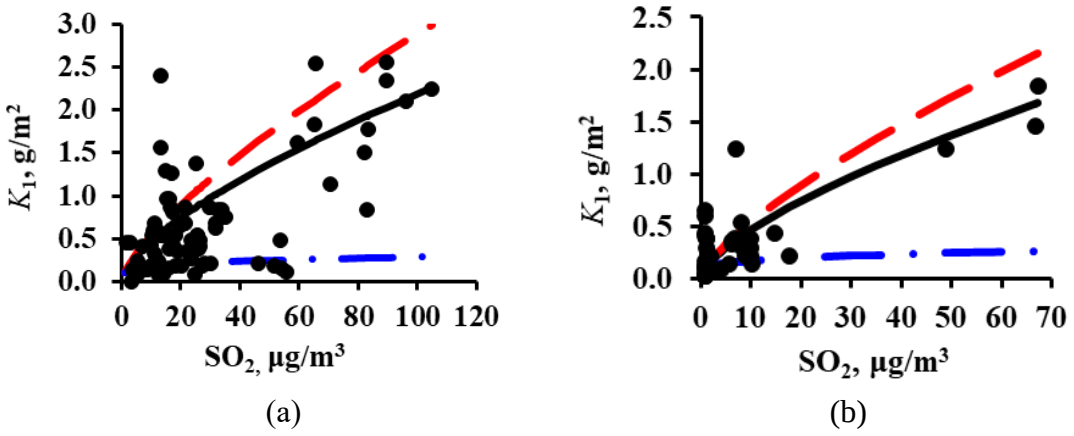

Figure 2. Plot of the first-year corrosion losses of aluminum (K_1) on SO_2 concentration based on the data from ISO CORRAG program (a) and MICAT project (b). ——: α = 0.67 (New DRF), — —: α = 0.73 (Standard DRF), — • —: α = 0.23 (Unified DRF).

In addition to the parameters mentioned above, the Unified DRFs include $[H^+]$—acidity of precipitation and $[O_3]$—ozone concentration for copper, as well as $[Cl^-]$—concentration of chlorides in rain water for aluminum. Ozone is certainly among the important parameters that affect the corrosion of metals. For example, it is noted that ozone can stimulate the formation of oxides and their effect on the protective properties of corrosion products [25,26]. Despite the importance of this factor in the estimation of corrosion effects, in reality the ozone concentration is only measured in a small number of locations. Data on $[H^+]$ and $[Cl^-]$ are also available for a small number of test locations. In view of this, these parameters are currently not used in the New DRFs.

The New DRFs developed for the prediction of K_1 (g/m^2) have the form:

For copper, Eq 6,

$$K_1 = 0.5\,[SO_2]^{0.38}\exp\{0.025\,RH + 0.085\,(T-10) + 0.0003\,Prec\},\ T \le 10\ ^\circ C;$$
$$K_1 = 0.5\,[SO_2]^{0.38}\exp\{0.025\,RH - 0.040\,(T-10) + 0.0003\,Prec\},\ T > 10\ ^\circ C \quad (6)$$

For aluminum, Eq 7,

$$K_1 = 0.01\,[SO_2]^{0.67}\exp\{0.039\,RH + 0.032\,(T-10) - 0.0001\,Prec\},\ T \le 10\ ^\circ C;$$
$$K_1 = 0.01\,[SO_2]^{0.67}\exp\{0.039\,RH - 0.065\,(T-10) - 0.0001\,Prec\},\ T > 10\ ^\circ C \quad (7)$$

The coefficient at *Prec* was found to be negative for aluminum. Attempts to use a positive coefficient for *Prec* with various combinations of other coefficients gave poorer results of K_1 prediction. It has been shown [26] that dust can accelerate the adsorption of moisture and SO_x from the atmosphere, which results in long-term surface acidification. Protective aluminum coatings are unstable under these conditions. Furthermore, carbon-containing dust can initiate pitting due to galvanic effects. Apparently, precipitations wash the dust off, thus favoring a decrease in aluminum corrosion, as the negative coefficient at *Prec* in Eq 7 shows. It should however be noted that the coefficient values and signs found by regression analysis may be unexplainable in a rational manner.

3.2. Screening the test locations for copper and aluminum K_1 prediction

The K_1 predictions for carbon steel and zinc [21] were also performed within the UN/ECE and RF programs and the MICAT project. The number of test locations (taking the number of exposures at each location into account) was 77 and 94 under the UN/ECE program, 63 and 61 under the MICAT program for steel and zinc, respectively, and 12 locations for each metal under the RF program. It was shown that for steel and zinc, some test locations under the MICAT project had considerably higher experimental K_1 values (K_1^{exp}) in comparison with the K_1 values predicted using various DRFs (K_1^{pr}). This regularity indicates a possible inaccuracy of K_1^{exp} or corrosivity parameters at these locations. Screening of these locations was not performed. These locations were attributed to locations with doubtful data.

Copper and aluminum have been tested in a smaller number of locations and with smaller number of exposures in these locations. The number of test locations for copper is 27 under the UN/ECE program and 61 under the MICAT program. Aluminum was not tested within the UN/ECE program. It was tested in 53 locations (the largest number of locations) under the MICAT project. For copper and aluminum, preliminary data screening was performed in the MICAT project for those locations where K_1^{pr} provided by various DRFs considerably differed from K_1^{exp} for steel and zinc [21]. These are the following locations: A3 (3 exposures), B1, B10, B11, B12, CO3 (3 exposures), and E5 (3 exposures) for copper, and additionally M3 (3 exposures) for aluminum. These locations are shown in italics in Table 3. After screening of the locations used in the MICAT project, 47 test locations remained for copper and 40 for aluminum. No screening of test locations was performed for copper data in the UN/ECE program.

3.3. K_1 predictions for copper using various DRFs

The K_1^{pr} results for copper obtained using the Standard DRF (Eq 1), Unified DRF (Eq 3), and the New DRF (Eq 6) are presented separately for each test program. To build the plots, the test locations were arranged in the order of increasing experimental K_1^{exp} values. Their sequence numbers are given in Tables 1–3. All the plots are drawn on the same scale. The plots show the prediction error lines $\delta = \pm 30\%$ (range: $1.3K_1^{exp}$–$0.7K_1^{exp}$). This provides a visual picture of how K_1^{pr} compares with K_1^{exp} for each DRF. No estimate on the difference between the K_1^{pr} values obtained using various DRFs and the K_1^{exp} values for each test locations within each program was made. The scatter of points is inevitable. It results from the imperfection of each DRF and the inaccuracy of experimental data on meteorological parameters, SO_2 content, and K_1^{exp} values. Let us just note the general regularities of the results on K_1^{pr} for each DRF.

The results on K_1^{pr} for copper under the MICAT project and the UN/ECE and RF programs are presented in Figures 3–5, respectively. It should be noted that the K_1^{pr} values for copper obtained using the Unified DRF (Eq 3) were quite insignificant. Apparently, like for carbon steel [21], the K_1^{pr} values were calculated in μm rather than in g/m^2 as the authors assumed. To convert K_1^{pr} in μm to K_1^{pr} in g/m^2, the prediction results were multiplied by 8.96, which corresponds to an 8.96-fold increase in the coefficients (0.0027 and 0.05) in Eq 3.

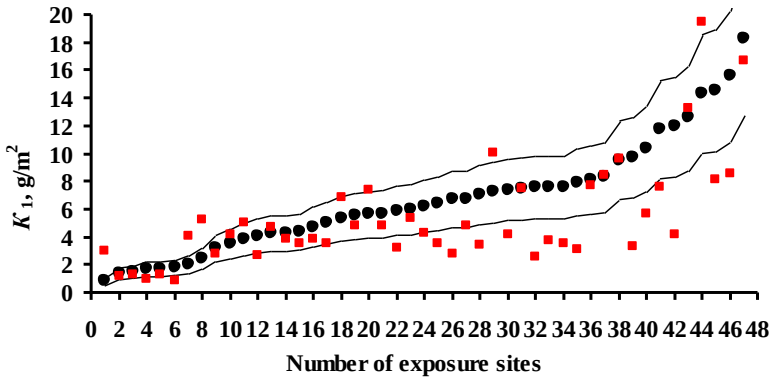

(a)

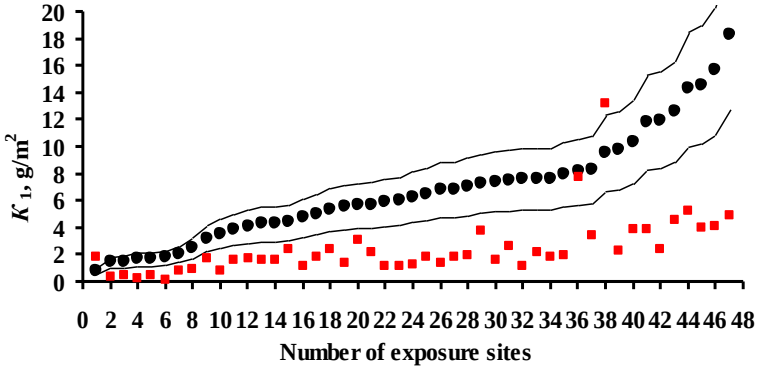

(b)

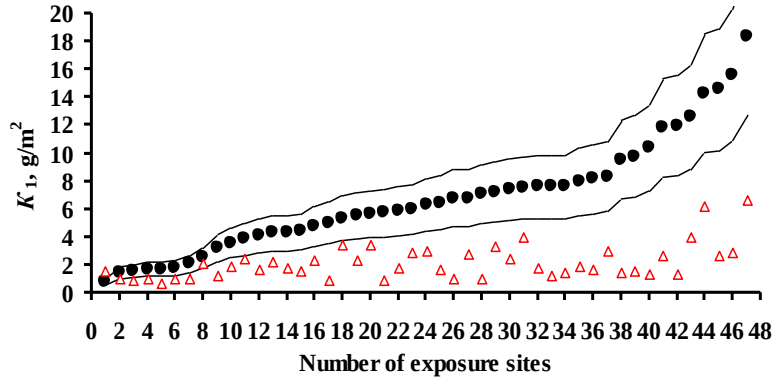

(c)

Figure 3. Copper. MICAT program. K_1 predictions by the New DRF (a), Standard DRF (b), and Unified DRF (c). ●: experimental data for K_1; ■: predictions for K_1; Δ: predictions for K_1 without consideration for ozone and *Rain* [H^+] (for Unified DRF only). Thin lines show the calculation error (±30%). The numbers correspond to the test locations as indicated in Table 2.

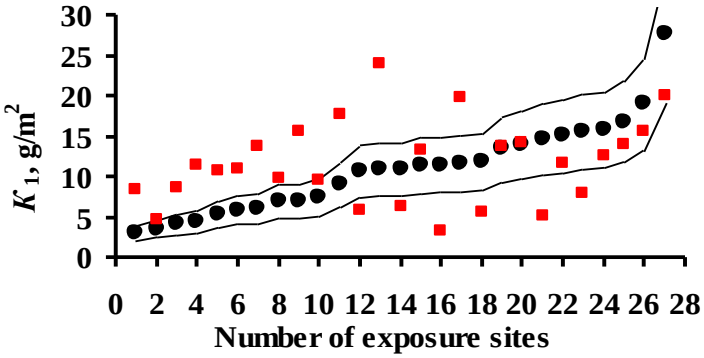

(a)

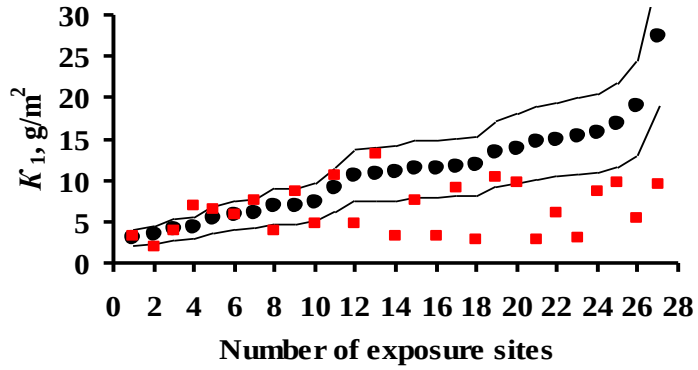

(b)

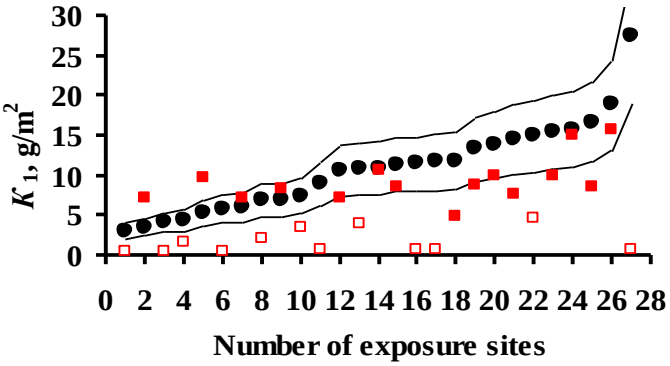

(c)

Figure 4. Copper. UN/ECE program. K_1 predictions by the New DRF (a), Standard DRF (b), and Unified DRF (c). ●: experimental data for K_1; ■: predictions for K_1; □: predictions for K_1 without consideration for ozone (for Unified DRF only). Thin lines show the calculation error (±30%). The numbers correspond to the test locations as indicated in Table 1.

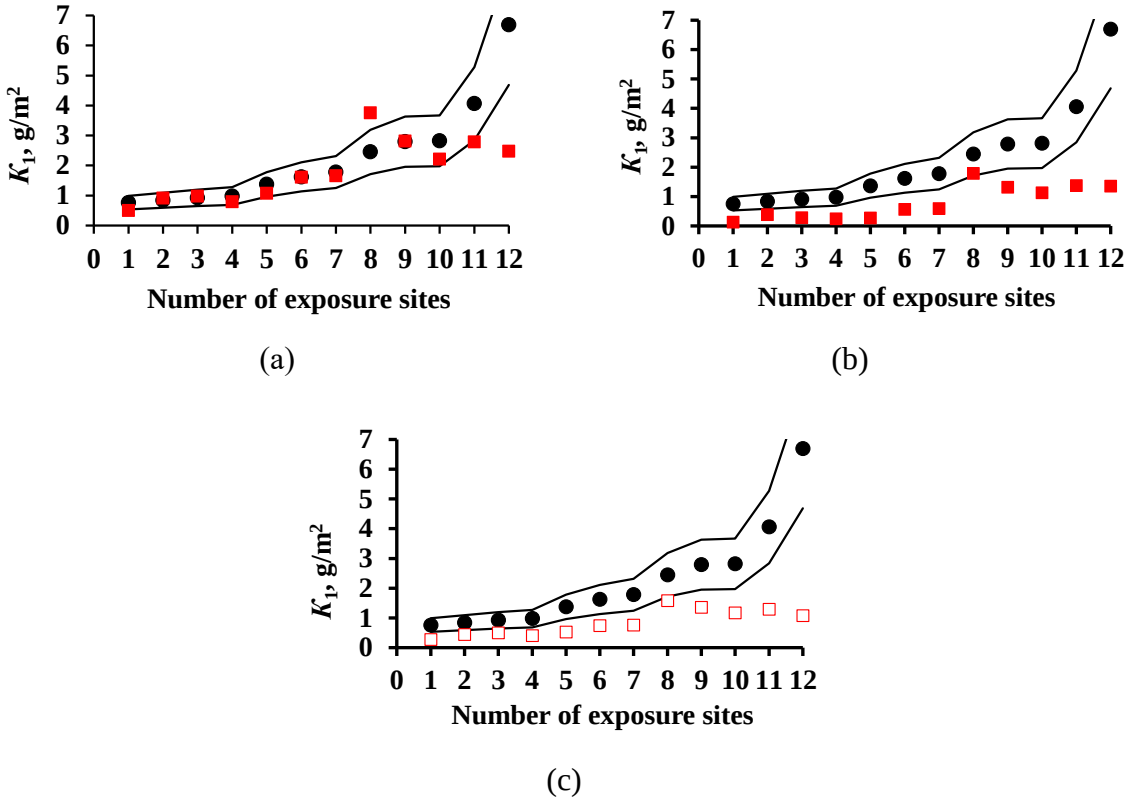

Figure 5. Copper. RF program. K_1 predictions by the New DRF (a), Standard DRF (b), and Unified DRF (c). ●: experimental data for K_1; ■: predictions for K_1; □: predictions for K_1 without consideration for ozone and *Rain* [H^+] (for Unified DRF only). Thin lines show the calculation error (±30%). The numbers correspond to the test locations as indicated in Table 3.

The K_1^{pr} values calculated by the New DRFs in the test locations of the MICAT project either lie in the range of δ = ±30% or are considerably underestimated in comparison with K_1^{exp}, Figure 3a, indicating that the prediction errors are distributed nonuniformly. As one can see in Figure 1c, many test locations with insignificant [SO_2] have high K_1^{exp} values. Perhaps, despite the preliminary screening, certain locations have unreasonably overestimated K_1^{exp} values. For locations within the UN/ECE program, the K_1^{pr} error has a symmetric distribution at first approximation, while there are few locations with K_1^{pr} within δ = ±30%, Figure 4a. It is evident from Figure 1b that the K_1^{exp} values at [SO_2] < 20 μg/m^3 are higher or much higher than those at [SO_2] > 20 μg/m^3. Taking into account that no screening of test locations used in the UN/ECE program was done, we present only a comparison of K_1^{exp} values, e.g., for SWE24 (No. 5), SWE25 (No. 4) and SWE26 (No. 12) (the test location numbers are given according to Table 1). Under practically equal climatic conditions, in SWE26 at [SO_2] = 3.3 μg/m^3, K_1^{exp} = 10.71 g/m^2, which is approximately two times higher than in SWE25 and SWE24: K_1^{exp} = 4.40 and 5.33 g/m^2 at higher [SO_2] concentrations of 19.6 and 16.8 μg/m^3, respectively. If K_1^{exp} were 4.40 or 5.33 g/m^2 at [SO_2] = 3.3 μg/m^3, and K_1^{exp} were 10.71 g/m^2 at [SO_2] = 19.6 or 16.8 μg/m^3, then K_1^{pr} would have matched K_1^{exp}. In these locations, the [O_3] values differ insignificantly according to data of other exposures [2,3] (these data are not

reported there since copper was not exposed in those periods). Therefore, it is hard to explain the observed difference in K_1^{exp} in these locations. It is possible that, apart from ozone, other parameters affecting copper corrosion were not taken into consideration, or not all locations in this program had reliable data. For locations under the RF program, except for 2 locations, nearly all K_1^{pr} values are within the $\delta = \pm 30\%$ range, Figure 5a. In total, the K_1^{pr} error is nearly symmetrical with respect to K_1^{exp}.

The K_1^{pr} values calculated by the Standard DRF for almost all the test locations are considerably lower than K_1^{exp}, Figure 3b. Under the UN/ECE program, the K_1^{pr} values for some locations are within the range of $\delta = \pm 30\%$, but for the other locations these values are considerably lower than K_1^{exp}, Figure 4b. In locations under the RF program, the K_1^{pr} values are also lower than K_1^{exp}, Figure 5b.

It is difficult to estimate K_1^{pr} using Unified DRF since no $[O_3]$ and $[H^+]$ data required for Eq 3 are available in many locations. Under the UN/ECE program, for the locations with a full set of parameters used in the DRFs, the K_1^{pr} errors are within the $\delta = \pm 30\%$ range or slightly exceed it, while if ozone is not taken into account, the K_1^{pr} values are considerably underestimated, Figure 4c. It should be noted that at $[O_3] = 27–77$ μg/m^3 (Table 1), K_1^{pr} can be increased 14–31 fold. Taking this effect of ozone into account, K_1^{pr} can be highly overestimated at some locations. In locations under the MICAT project and RF program, the K_1^{pr} values are also lower than K_1^{exp}, Figure 5c, due to the lack of $[O_3]$ data (MICAT project) or both $[O_3]$ and $[H^+]$ data (RF program). The corrosion losses due to the acidity of precipitation (ΔK_1^{H+}) in Eq 3 are taken into account by a separate component. For example, the ΔK_1^{H+} value can reach 11.8 g/m^2 at US39 (No. 26, UN/ECE program). Comparison of K_1^{pr} and K_1^{exp} allows one to assume that in an atmosphere contaminated with SO_2, ozone and acidic precipitations affect corrosion more significantly than SO_2, but we believe this to be unlikely. Let us remind the reader that we increased the K_1^{pr} results obtained by Eq 3 by a factor of 8.96.

Comparison of the K_1^{pr} results for all DRFs with K_1^{exp} indicates that none of the models is perfect. New tests are required for copper, with simultaneous recording of meteorological and aerochemical parameters that affect copper corrosion. Let us just note that currently the New DRFs give the most reliable K_1^{pr} values in comparison with the K_1^{pr} values calculated by the Standard DRF and Unified DRF.

3.4. Analysis of DRFs for copper

The DRFs were analyzed by comparison of the coefficients used in these DRFs. The nonlinear New DRFs (Eq 6) and Standard DRFs (Eq 1) can be represented in the form:

$$K_1 = A\,[SO_2]^{\alpha}\exp\{k_1 \cdot RH + k_2\,(T-10) + k_3 \cdot Prec\} = K_1^{0}\,[SO_2]^{\alpha} \tag{8}$$

where $K_1^{0} = A\exp\{k_1 \cdot RH + k_2\,(T-10) + k_3 \cdot Prec\}$.

Unified DRFs (Eq 3) can be presented in the form:

$$K_1 = A\,[SO_2]^{\alpha}\,[O_3]^{\beta} \cdot RH\exp\{k_2\,(T-10)\} + B \cdot Rain\,[H^+];$$

$$\text{or } K_1 = A\,[SO_2]^{\alpha}\,[O_3]^{\beta} \cdot RH \cdot \exp\{k_2\,(T-10)\} + B \cdot Rain\,[H^+] \approx K_1^{0}\,[SO_2]^{\alpha} \tag{9}$$

where $K_1^0 = A\ [O_3]^{\beta} \cdot RH \cdot \exp\{k_2\ (T - 10)\}$, provided that ozone is considered to be a parameter of pure atmosphere and that the $B \cdot Rain\ [H^+]$ member can be neglected.

The values of the coefficients used in Eqs 1, 3 and 6 are presented in Table 4.

Table 4. The values of coefficients used in DRF for copper.

DRF	A		α	β	k_1	k_2		k_3	B	
	μm	g/m^2				$T \le 10$ °C	$T > 10$ °C		μg	g/m^2
New	0.0558	0.50	0.38	-	0.025	0.085	−0.040	0.0003	-	-
Standard	0.0053	0.047	0.26	-	0.059	0.126	−0.080	-	-	-
Unified	0.0027	0.024	0.32	0.79	-	0.083	−0.032	-	0.050	0.448

To compare the $[SO_2]^{\alpha}$ plots, with the α values taken into account for all DRFs, Eq 5 used K_1^0 = 3 g/m^2 at $[SO_2]$ = 1 μg/m^3, which at first approximation corresponds to an average K_1 value in a pure atmosphere for the entire set of experimental data. The plots for all the programs are presented in Figure 1. For the New DRF, the line $K = f([SO_2])$ at α = 0.38 passes approximately through the mean experimental points from all the test programs. Therefore, one should expect a relatively uniform distribution of prediction errors (Figures 3a, 4a and 5a). For the Standard DRF, α = 0.26 is somewhat lowered, which may result in a small K_1 range as a function of $[SO_2]$, i.e., in underestimated K_1^{pr} values, especially at high $[SO_2]$ (Figures 3b, 4b and 5b). For Unified DRF, α = 0.32 is slightly underestimated. However, with a full set of corrosivity parameters in Eq 3, the K_1^{pr} values match K_1^{exp} at first approximation (Figure 4c), which may be due to a combined effect of other parameters, e.g., due to $\Delta K_1^{H+} = B \cdot Rain\ [H^+]$.

To perform a comparative estimate of k_1 and k_2, let us use the value where a change in the temperature dependence is observed, i.e., T_{lim} = 10 °C accepted in the DRF. Let us assume that at T_{lim} = 10 °C and the most common RH = 75%, K_1 = 3 g/m^2. The dependences of K on T and RH under these conditions and with consideration for the corresponding k_1 and k_2 values for each DRF are presented in Figure 6.

According to the New DRF (k_1 = 0.025), K may decrease from 3 to 0.97 g/m^2 upon RH change from 75 to 30%, while an increase in RH to 100% increases K to 5.61 g/m^2, i.e., K changes 5.8-fold upon RH variation from 30 to 100% (Figure 6a). For the Standard DRF (k_1 = 0.059), K changed abruptly, i.e., it increases 62-fold upon RH variation from 30 to 100%. In Unified DRF (Eq 3), K linearly depends on RH, hence K can increase 3.3-fold in the same range of RH variation.

For all the DRFs, the absolute value of k_2 is larger at $T \le 10$ °C than at $T > 10$ °C, i.e., K decreases more abruptly upon a temperature decrease than upon its increase from 10 °C (Figure 6b). According to the Standard DRF, the most abrupt decrease should be observed for two temperature ranges. At k_2 = 0.126 and −0.080, the K value decreases from 3 to 0.09 g/m^2 (upon temperature decrease to −18 °C) and to 0.61 g/m^2 (upon temperature increase to 30 °C). This corresponds to 33- and 6.8-fold K decrease, respectively.

The nonlinear effect of $Prec$ on corrosion is only taken into account in the New DRF. This effect is represented using EC2 data (MICAT project): at T = 12.9 °C, RH = 66%, $[SO_2]$ = 1 μg/m^3 and $Prec$ = 554 mm/y, K_1 equals 3.2 g/m^2. A change in $Prec$ from 500 to 2500 mm/y at k_3 = 0.0003

can increase K to 6 g/m^2, i.e., almost twofold, Figure 6c. The effect of O_3 was only used in Unified DRF, Figure 6d. Owing to O_3, in locations with climate conditions similar to SPA33 (UN/ECE program, T = 14 °C, RH = 64%, $Prec$ = 785 mm/y, [SO_2] = 3.3 μg/m^3, [O_3] = 77 μg/m^3), variation of O_3 concentration from 10 to 100 μg/m^3 can increase K 6-fold (at β = 0.79). In Unified DRF, the separate contribution of $\Delta K_1^{H+} = B \cdot Rain \cdot [H^+]$ to corrosion linearly depends on $Rain$ and [H^+]. It is known that in case of a linear dependence, a combination of high constituent values can result in a high ΔK_1^{H+} value.

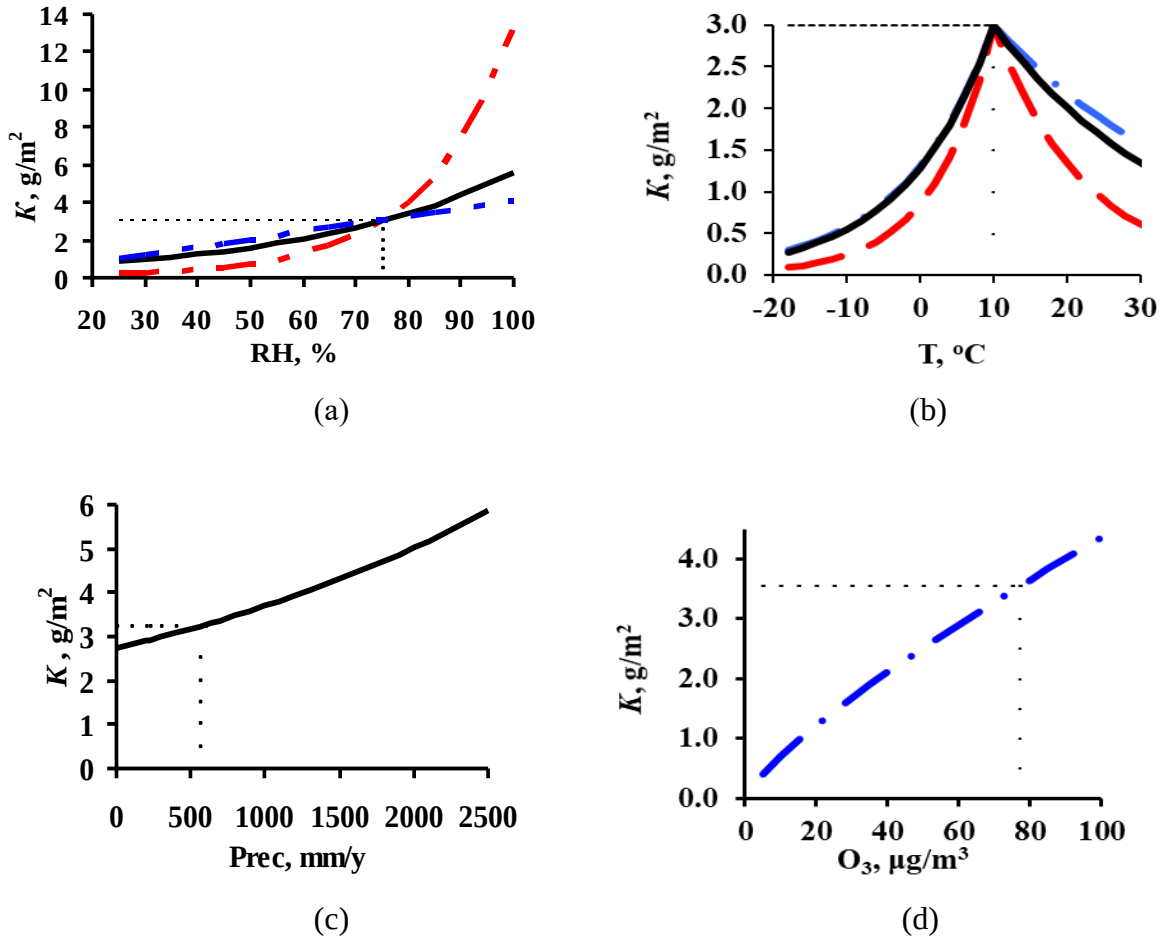

Figure 6. Variation of K for copper *versus* relative humidity (a), temperature (b), precipitations (c), and ozone concentration (d) with account for the values of the DRF coefficients. ——— by the New DRF; — — — by the Standard DRF; —·— by the Unified DRF.

The A values are 0.50 in the New DRFs and 0.047 and 0.024 g/m^2 in the Standard DRF and Unified DRF, respectively, i.e., the A values differ 10.6- and 20.8-fold.

It has been shown that the K_1^{pr} values obtained for copper using DRFs with different parameters affecting corrosion and/or their combinations are taken into account, as well as having different coefficients at similar parameters, differ considerably, Figures 3–5.

3.5. K_1 predictions for aluminum using various DRFs

The difficulty of K_1 prediction for aluminum lies in the possibility that large errors in K_1^{exp} determination may have to be tolerated. For example, the K_1^{exp} values in a pure atmosphere may lie within the experimental error due to the complexity of removal of corrosion products from pits, etc. Under the same test conditions, the variation of K_1^{exp} is many times greater than for other metals. For example, in the MICAT project, the K_1^{exp} values vary 68-fold for aluminum (0.027–1.836 g/m^2) but only 23-fold for copper. It is more difficult to predict such differences using the same parameters in the DRFs.

The K_1^{pr} results for aluminum obtained using the Standard DRF (Eq 2), Unified DRF (Eq 4), and the New DRF (Eq 7) are presented separately for each test program. To build the plots, the test locations were arranged in the order of increasing K_1^{exp} values. Their sequence numbers are given in Tables 2 and 3. The plots are built on the same scale. They show the prediction error lines $\delta = \pm 30\%$ (range: $1.3K_1^{exp}$–$0.7K_1^{exp}$). The results on K_1^{pr} for locations used in the MICAT project and the RF program are presented in Figures 7 and 8, respectively. Notwithstanding the preliminary screening in the MICAT project, let us additionally compare the K_1^{exp} values obtained in a number of locations. For example, in the pure atmosphere in PE4 (No. 1 and 2, Table 2) at low *RH* (37 and 33%) and *Prec* values (17 and 34 mm/y), the K_1^{exp} value amounts to 0.027g/m^2. The same K_1^{exp} value was obtained in PE5, PE6, and U1 locations (No. 3, 4, 5, 6, respectively, Table 2) at higher *RH* (67–83%) and *Prec* values (632–1324 mm/y), which is hardly possible. Thus, it follows that the experimental data in some other locations are also doubtful.

Let us note the general regularities of the results on K_1^{pr} for each DRF.

For locations under the MICAT project, the K_1^{pr} values calculated using the New DRFs fit in the range $\delta = \pm 30\%$ and are either under- or overestimated in comparison with K_1^{exp}, Figure 7a. At first approximation, the K_1^{pr} error has a symmetric distribution. Overestimated K_1^{pr} values are mainly observed in locations with K_1^{exp} within 0–0.2 g/m^2, whereas underestimated K_1^{pr}—at locations with higher K_1^{exp}. For locations under the RF program, except for one location, nearly all K_1^{pr} values are within the $\delta = \pm 30\%$ range, Figure 8a. In total, the K_1^{pr} error is nearly symmetrical with respect to K_1^{exp} for both programs.

The K_1^{pr} values calculated by the Standard DRF lie in the range $\delta = \pm 30\%$ for the test locations under the MICAT project only at K_1^{exp} up to 0.2 g/m^2, Figure 7b. For the other locations, the K_1^{pr} values are lower or much lower than K_1^{exp}. For locations under the RF program, the K_1^{pr} values are also underestimated in comparison with K_1^{exp}, Figure 8b.

In the K_1^{pr} values obtained using Unified DRF, the component of corrosion losses due to the content of chlorides in deposits, $\Delta K_1^{Cl^-}$, is not taken into account. Without this component, the mainly underestimated K_1^{pr} values manifest themselves as a nearly horizontal band for both programs, Figures 7c and 8c. Hence higher K_1^{pr} values in an atmosphere contaminated with SO_2 can be obtained only from the presence of chloride ions in deposits, which is unlikely for continental territories.

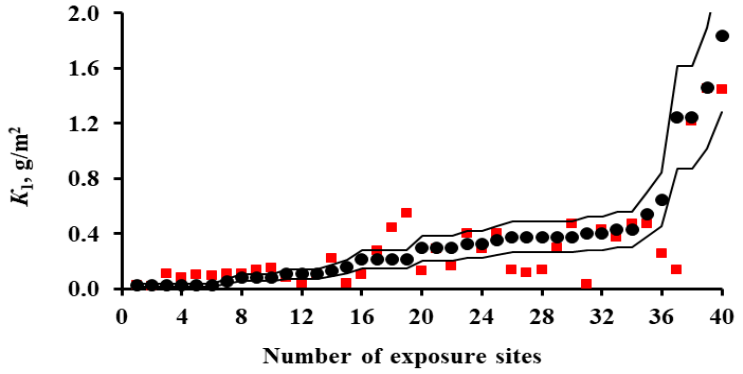

(a)

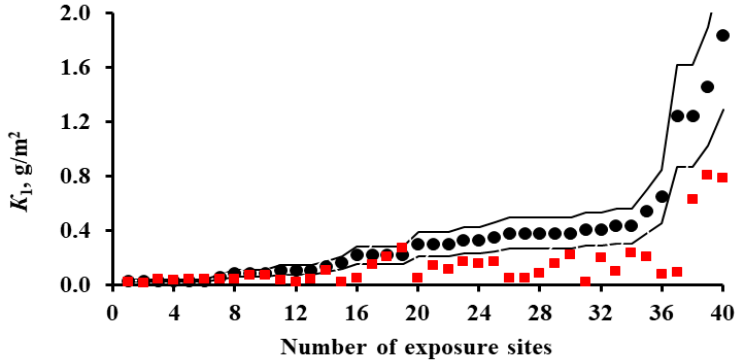

(b)

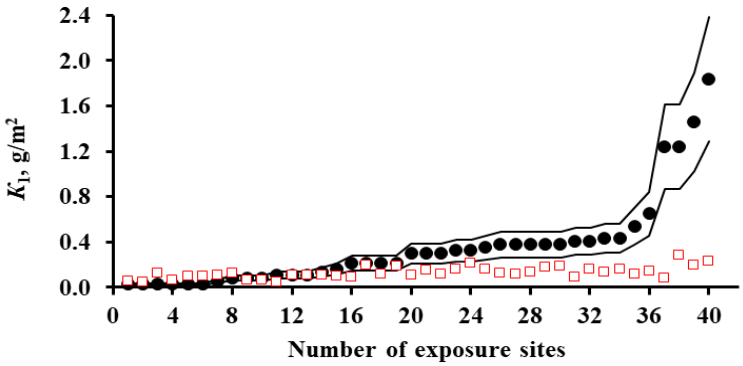

(c)

Figure 7. Aluminum. MICAT program. K_1 predictions by the new DRF (a), Standard DRF (b), and Unified DRF (c). ●: experimental data for K_1; ■: – predictions for K_1; □: predictions for K_1 without consideration for *Rain* [Cl^-] (for Unified DRF only). Thin lines show the calculation error (±30%). The numbers correspond to the test locations as indicated in Table 2.

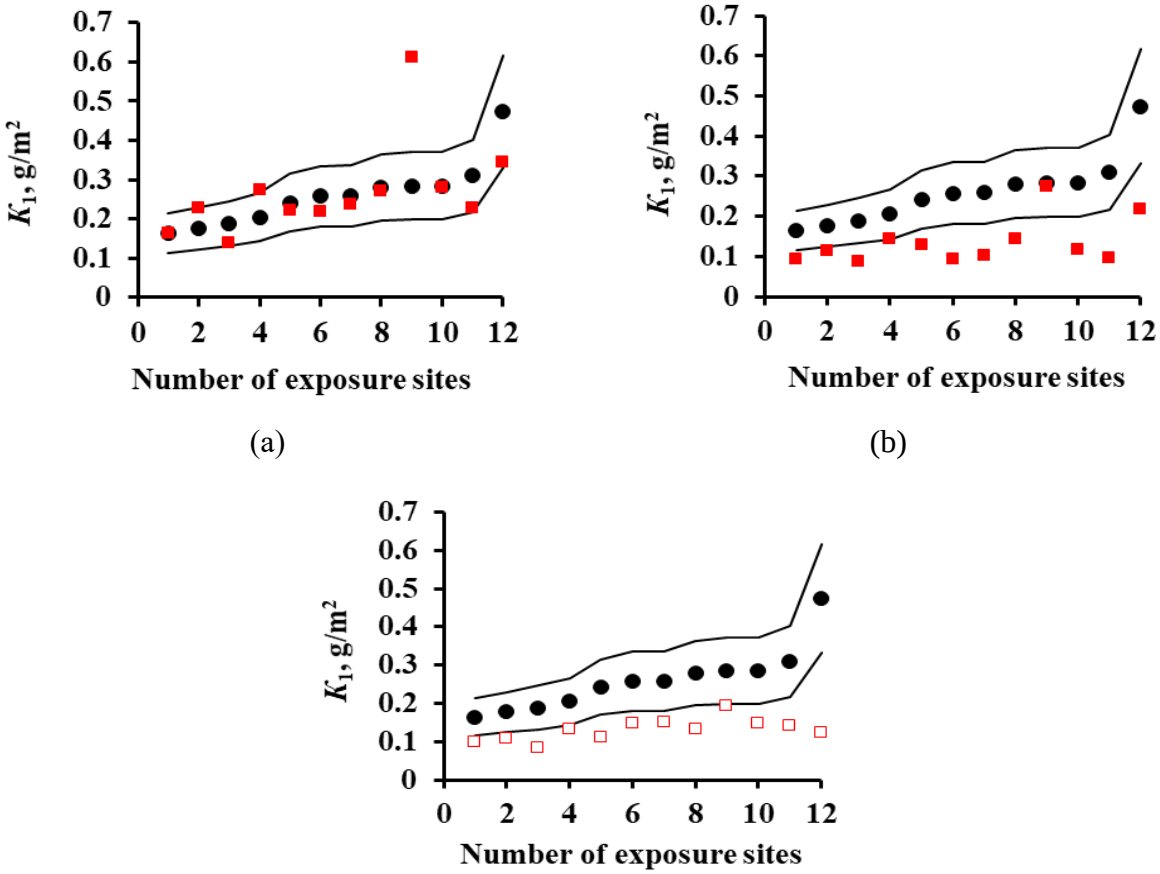

Figure 8. Aluminum. RF program. K_1 predictions by the new DRF (a), standard DRF (b), and Unified DRF (c). ●: experimental data for K_1; ■: predictions for K_1; □: predictions for K_1 without consideration for *Rain* {Cl^-] (for Unified DRF only). Thin lines show the calculation error (±30%). The numbers correspond to the test locations as indicated in Table 3.

In the MICAT project, data on the concentration of chlorides in deposits are unavailable. Therefore, to estimate the possible ΔK_1^{Cl-} value, let us use the data on chloride concentration in precipitates for locations under the UN/ECE program. Of all test locations under this program, with insignificant salt content in the atmosphere (1.5 mg/(m^2 day)) in Waldhof Langenbrügge GER7, the highest chloride concentration in the precipitates is [Cl^-] = 3.92 mg/L, Table 1. This value is applicable for K_1^{pr} calculations in two locations: Brazil, Belem, B8 (T = 26.1 °C, RH = 88% *Rain* = 2395 mm/y, [SO_2] = Ins, [Cl^-] = Ins., Table 2) and Brazil, Sao Paulo, B6 (T = 19.5 °C, RH = 76%, *Rain* = 1810 mm/y, [SO_2] = 66.75 μg/m^3 and [Cl^-] = Ins., Table 2). In these locations, K_1^{exp} amounted to 0.378 g/m^2 and 1.458 g/m^2, respectively. The K_1^{exp} were 0.378 g/m^2 and 1.458 g/m^2, respectively, in these locations. The K_1^{pr} values determined using Eq 4 with consideration for corrosion due to chlorides in rain water (ΔK_1^{Cl-}) at [Cl^-] = 3.92 mg/L were found to be 0.126 + 0.582 = 0.708 g/m^2 in Belem and 0.195 + 0.440 = 0.635 g/m^2 in Sao Paulo. In the pure atmosphere of Belem, K_1^{pr} can match K_1^{exp} due to the ΔK_1^{Cl-} component at a lower chloride concentration in the

precipitation, while ΔK_1^{Cl-} predominates in the overall corrosion effect. In Sao Paulo, even taking the ΔK_1^{Cl-} component into account, the K_1^{pr} value is 2.3 times higher than K_1^{exp}, though the [Cl^-] amount in the precipitation is the largest among the continental territories.

Comparison of the K_1^{pr} values with K_1^{exp} for all the DRFs indicates that the New DRFs currently give the most reliable K_1^{pr} values in comparison with the K_1^{pr} values calculated by the Standard DRF and Unified DRF.

3.6. Analysis of DRFs for aluminum

The DRFs were analyzed by comparison of the coefficients used in these DRFs. The nonlinear New DRFs (Eq 7) and Standard DRFs (Eq 2) can be represented in the form: New DRFs (Eq 6) and Standard DRFs (Eq 1) can be represented in the form:

$$K_1 = A\ [SO_2]^{\alpha}\ \exp\{k_1\ RH + k_2\ (T - 10) + k_3\ Prec\} = K_1^{0}\ [SO_2]^{\alpha} \tag{10}$$

where $K_1^{0} = A\ \exp\{k_1\ RH + k_2\ (T - 10) + k_3\ Prec\}$.

Unified DRF (Eq 4) can be represented as:

$$K_1 = A\ [SO_2]^{\alpha}\ RH\ \exp\{k_2\ (T - 10)\} + B\ Rain\ [Cl^-] \approx K_1^{0}\ [SO_2]^{\alpha} \tag{11}$$

where $K_1^{0} = A\ RH\ \exp\{k_2\ (T - 10)\}$, provided that $B\ Rain\ [Cl^-] = 0$ in SO_2-containing atmospheres, which is only possible at [Cl^-] = 0.

The values of the coefficients used in Eqs 2, 4, and 7 are presented in Table 5.

Table 5. The values of coefficients used in DRF for aluminum.

DRF	*A*		α	k_1	k_2		k_3	*B*	
	μm	g/m^2			$T \leq 10$ °C	$T > 10$ °C		μg	g/m^2
New	0.0037	0.010	0.67	0.039	0.032	−0.065	−0.0001	-	-
Standard	0.0042	0.0113	0.73	0.025	0.009	−0.043	-	-	-
Unified	0.00078	0.0021	0.23	-	0.031	−0.061	-	0.000023	0.000062

To compare the K–[SO_2]$^{\alpha}$ plots with the α values for all the DRFs taken into account, in Eq 5 we used K_1^{0} = 0.1 g/m^2 at [SO_2] = 1 μg/m^3, which at first approximation corresponds to the average K_1 value in a pure atmosphere for the entire set of experimental data. These plots for the test locations under all the programs are presented in Figure 2. For the new DRF, the $K = f([SO_2])$ line at α = 0.67 passes approximately through the mean experimental points of all the test programs. Therefore, one should expect a relatively uniform distribution of prediction errors (Figures 7a and 8a). The value for the Standard DRF, α = 0.73, is somewhat overestimated. The value for Unified DRF, α = 0.23, is considerably underestimated. This α value makes it impossible to obtain a large K_1^{pr} variation range. As a result, K_1^{pr} is considerably smaller than K_1^{exp} (Figures 7c and 8c), thus the mass losses had to be increased by adjusting other atmosphere corrosivity parameters.

Let us make a comparative estimate of k_1 and k_2, assuming that K_1 = 0.1 g/m^2 at T = 10 °C and RH = 75%. The plots of K vs. T and RH under these conditions and with consideration for the corresponding k_1 and k_2 for each DRF are presented in Figure 9.

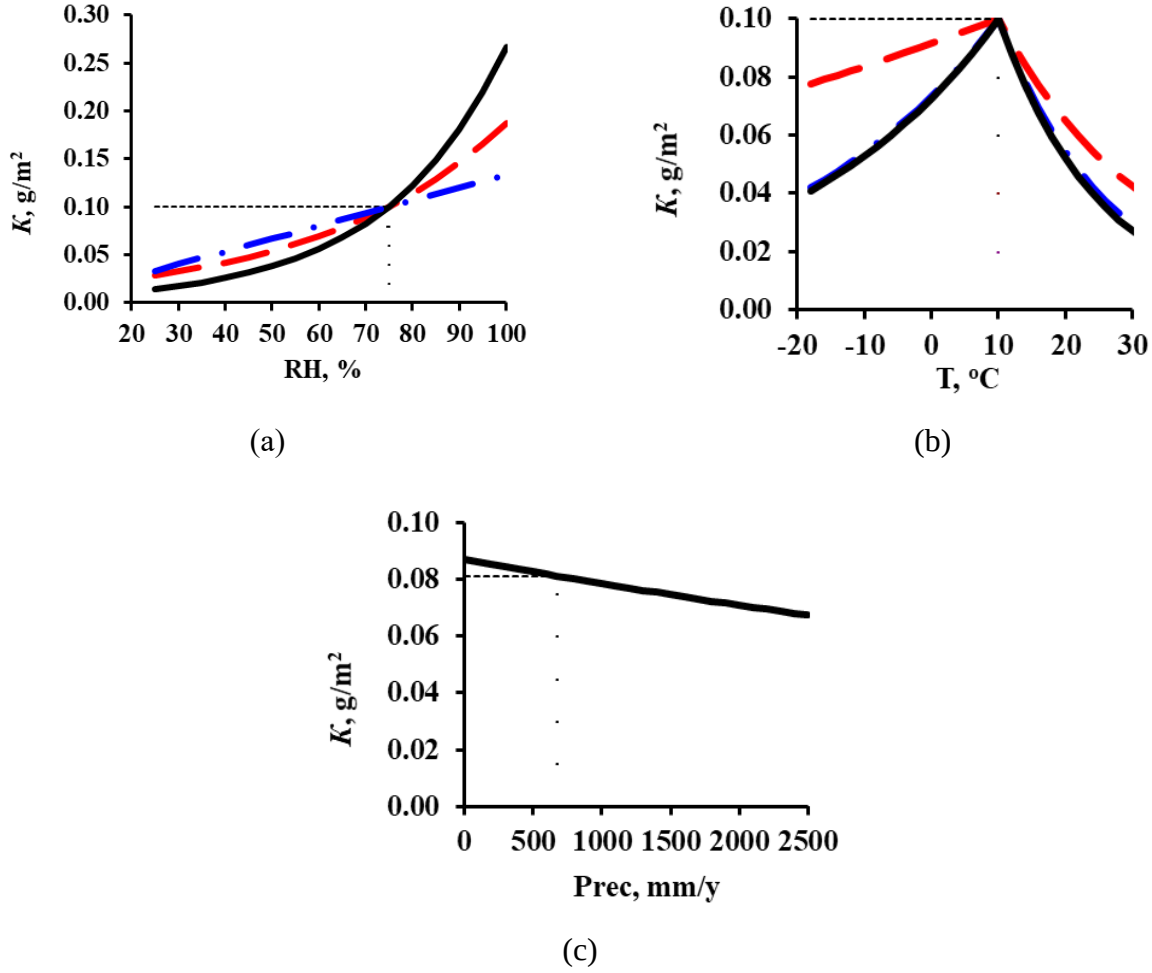

Figure 9. Variation of K for aluminum *versus* relative humidity (a), temperature (b) and precipitations (c) with account for the values of the DRF coefficients. ——— by the new DRF; — — by the Standard DRF; —·— by the Unified DRF.

In the New DRF, the effect of RH (k_1 = 0.039) on corrosion is higher than in the other DRFs. On RH variation from 30 to 100%, K can increase from 0.014 to 0.266 g/m^2, in the Standard DRF (k_1 = 0.025) from 0.033 to 0.188 g/m^2, whereas in Unified DRF (linear K–RH relationship) K should increase 3.3-fold, i.e., from 0.04 to 0.133 g/m^2.

The effect of temperature on corrosion at $T \leq 10$ is weaker in the Standard DRF, k_2 = 0.009. This corresponds to a K decrease from 0.1 to 0.08 g/m^2 upon a T decrease from 10 °C to −18 °C. A strong temperature effect is expected by the New DRF (k_2 = 0.032) and Unified DRF (k_2 = 0.031): under the same conditions, K decreases from 0.1 to 0.04 g/m^2, respectively. A temperature increase from 10 to 30 °C results in an abrupt K decrease to 0.021, 0.023 and 0.036g/m^2 according to the New DRF (k_2 = −0.065), Unified DRF (k_2 = 0.061) and Standard DRF (k_2 = −0.043).The adverse effect of

Prec on corrosion is only taken into account in the New DRF. This relationship was presented using data from PE5 (MICAT project, at T = 12.2 °C, RH = 67%, $[SO_2]$ = 1 μg/m^3 and *Prec* = 672 mm/y, K_1 = 0.081 g/m^2). A change in *Prec* from 500 to 2500 mm/y at k_3 = −0.0001 can decrease K from 0.083 to 0.067 g/m^2, i.e., 1.2-fold, Figure 9c. For Unified DRF, the separate contribution of ΔK_1^{Cl-} = $B \cdot Rain \cdot [Cl^-]$ to mass losses linearly depends on *Rain* and the $[Cl^-]$ concentration therein.

The A values are 0.010, 0.0113 and 0.0021 g/m^2 in the New, Standard and Unified DRF, respectively. The A value differs 0.88- and 4.8-fold in comparison with the New DRFs.

The K_1^{pr} values obtained for each DRF using the presented combinations of considerably different coefficients for parameters affecting corrosion are shown in Figures 7 and 8.

4. Conclusions

1. The $K = f([SO_2])$ relationships for corrosion losses of copper and aluminum *vs*. sulfur dioxide concentration have been obtained.
2. Based on the $K = f([SO_2])$ relationships obtained, new DRFs for copper and aluminum have been developed for continental territories.
3. The predicted corrosion losses of copper and aluminum in the first year of exposure using the New DRF, Standard DRF, and Unified DRF are compared with experimental data for continental test locations under the UN/ECE, RF programs and MICAT project.
4. An analysis of the values of the coefficients used in the DRFs for the prediction of corrosion losses of copper and aluminum is presented. It is shown that the most accurate DRFs can only be developed based on the knowledge about the effects of each atmosphere corrosivity parameter on corrosion. Using this knowledge, it is possible to correctly choose the analytical form of the DRF, the coefficients in it, and to develop the most perfect DRFs.

Conflicts of interest

The authors declare no conflict of interest.

References

1. Knotkova D, Kreislova K, Dean SW (2010) ISOCORRAG International Atmospheric Exposure Program: Summary of Results, ASTM Series 71, West Conshohocken, PA: ASTM International.
2. Tidblad J, Kucera V, Mikhailov AA (1998) Statistical analysis of 8 year materials exposure and acceptable deterioration and pollution levels, In: *UN/ECE ICP on Effects on Materials, Report No. 30*, Stockholm, Sweden: Swedish Corrosion Institute, 1–49.
3. Tidblad J, Kucera V, Mikhailov AA, et al. (2001) UN ECE ICP Materials: Dose-Response Functions on Dry and Wet Acid Deposition Effects After 8 Years of Exposure. *Water Air Soil Poll* 130: 1457–1462.
4. Morcillo M, Almeida EM, Rosales BM, et al. (1998) Functiones de Dano (Dosis/Respuesta) de la Corrosion Atmospherica en Iberoamerica, In: *Corrosion y Proteccion de Metales en las Atmosferas de Iberoamerica*, Madrid, Spain: Programma CYTED, 629–660.

5. Morcillo M (1995) Atmospheric corrosion in Ibero-America: The MICAT project, In: Kirk WW, Lawson HH, *Atmospheric corrosion, ASTM STP 1239*, Philadelphia, PA: American Society for Testing and Materials, 257–275.
6. Panchenko YM, Shuvakhina LN, Mikhailovsky YN (1982) Atmospheric corrosion of metals in Far Eastern regions. *Zashchita metallov* 18: 575–582 (in Russian).
7. ISO 9223:2012(E) (2012) Corrosion of metals and alloys—Corrosivity of atmospheres—Classification, determination and estimation. International Standards Organization, Geneva.
8. Syed S (2006) Atmospheric corrosion of materials. *Emir J Eng Res* 11: 1–24.
9. De la Fuente D, Castano JG, Morcillo M (2007) Long-term atmospheric corrosion of zinc. *Corros Sci* 49: 1420–1436.
10. Landolfo R, Cascini L, Portioli F (2010) Modeling of metal structure corrosion damage: A state of the art report. *Sustainability* 2: 2163–2175.
11. Morcillo M, De la Fuente D, Diaz I, et al. (2011) Atmospheric corrosion of mild steel. *Rev Metal* 47: 426–444.
12. De la Fuente D, Diaz I, Simancas J, et al. (2011) Long-term atmospheric corrosion of mild steel. *Corros Sci* 53: 604–617.
13. Morcillo M, Chico B, Diaz I, et al. (2013) Atmospheric corrosion data of weathering steels: A review. *Corros Sci* 77: 6–24.
14. Surnam BYR, Chiu CW, Xiao HP, et al. (2015) Long-term atmospheric corrosion in Mauritius. *Corros Eng Sci Techn* 50: 155–159.
15. Panchenko YM, Marshakov AI, Igonin TN, et al. (2014) Long-term forecast of corrosion mass losses of technically important metals in various world regions using a power function. *Corros Sci* 88: 306–316.
16. Panchenko YM, Marshakov AI (2016) Long-term prediction of metal corrosion losses in atmosphere using a power-linear function. *Corros Sci* 109: 217–229.
17. ISO 9224:2012(E) (2012) Corrosion of metals and alloys—Corrosivity of atmospheres—Guiding values for the corrosivity categories. International Standards Organization, Geneva.
18. Tidblad J, Mikhailov AA, Kucera V (1999) Unified Dose-Response Functions after 8 Years of Exposure. *Quantification of Effects of Air Pollutants on Materials, UN ECE Workshop Proceedings*, Umweltbundesamt, Berlin, 77–86.
19. Tidblad J, Mikhailov AA, Kucera V (2000) Acid deposition effects on materials in subtropical and tropical climates. Data compilation and temperate climate comparison, KI Report, Stockholm, Sweden: Swedish Corrosion Institute, 1–33.
20. Chico B, De la Fuente D, Díaz I, et al. (2017) Annual atmospheric corrosion of carbon steel worldwide. An integration of ISOCORRAG, ICP/UNECE and MICAT databases. *Materials* 10: 601.
21. Panchenko YM, Marshakov AI (2017) Prediction of first-year corrosion losses of carbon steel and zinc in continental regions. *Materials* 10: 422.
22. Tidblad J, Mikhailov AA, Kucera V (2000) Model for the prediction of the time of wetness from average annual data on relative air humidity and air temperature. *Prot Metal* 36: 533–540.
23. Feliu S, Morcillo M, Feliu Jr S (1993) The prediction of atmospheric corrosion from meteorological and pollution parameters—I. Annual corrosion. *Corros Sci* 34: 403–414.

24. Mikhailov AA, Panchenko YM, Kuznetsov YI (2016) *Atmospheric corrosion and protection of metals*, Tambov: Pershin, Inc. (in Russian).
25. Zakipour S, Tidblad J, Leygraf C (1995) Atmospheric Corrosion Effects of SO_2 and O_3 on Laboratory-Exposed Copper. *J Electrochem Soc* 142: 757–760.
26. Tidblad J, Kucera V (1993) The role of NO_x and O_3 in the corrosion and degradation of materials, Report 1993:6E, Stockholm, Sweden: Swedish Corrosion Institute, 1–46.

AIMS Press